Supplementary material

S1. Flow tubes design

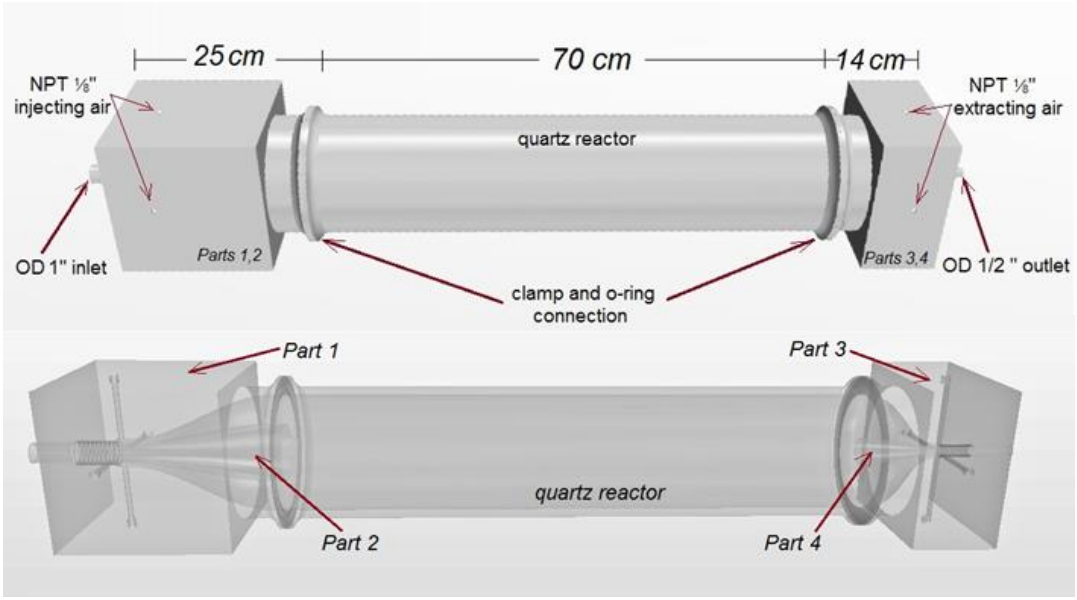

Figure S1. Design of the OPR flow tubes

S2. Assessment of potential measurement biases

Table S1. Average and peak values of O_3, NO_x, total VOCs, OH reactivity, $J(NO_2)$ and $J(O^1D)$, as well as timing of the peaks, for the selected days of the MCMA–2006 and the CalNex–2010 field campaigns.

Species		MCMA–2006		CalNex–2010	
		19 March 2006 9:00 – 18:00	**21 March 2006** 8:30 – 18:30	**30 May 2010** 8:00 – 18:30	**08 June 2010** 8:00 – 18:30
O_3 (ppbv)	average	40.9	73	69.8	35.0
	max	47.9	119.7	108.7	46.4
	peak timing	11:10	16:50	13:45	15:30
NO_2 (ppbv)	average	10.8	24.8	8.0	13.2
	max	36.3	69.9	14.3	20.3
	peak timing	09:00	09:10	11:45	12:45
NO (ppbv)	average	5.1	10.0	2.1	5.2
	max	18.8	61.5	5.1	13.2
	peak timing	09:00	8:30	08:15	12:45
Total VOCs (ppbv)	average	56.4	165.0	43.2	47.1
	max	148.5	331.8	49.6	68.0
	peak timing	09:00	08:30	11:30	13:00
OH reactivity (s^{-1})	average	12.9	35.8	14.6	14.9
	max	35.7	86.3	17.8	22.3
	peak timing	09:00	08:30	11:30	13:00
$J(NO_2)$ (s^{-1})	average	7.2×10^{-3}	5.2×10^{-3}	6.3×10^{-3}	5.6×10^{-3}
	max	9.8×10^{-3}	9.2×10^{-3}	7.8×10^{-3}	8.4×10^{-3}
	peak timing	12:40	12:40	13:15	11:15
$J(O^1D)$ (s^{-1})	average	2.7×10^{-5}	1.9×10^{-5}	1.6×10^{-5}	1.6×10^{-5}
	max	4.8×10^{-5}	4.3×10^{-5}	2.7×10^{-5}	2.9×10^{-5}
	peak timing	12:30	12:40	12:45	12:30

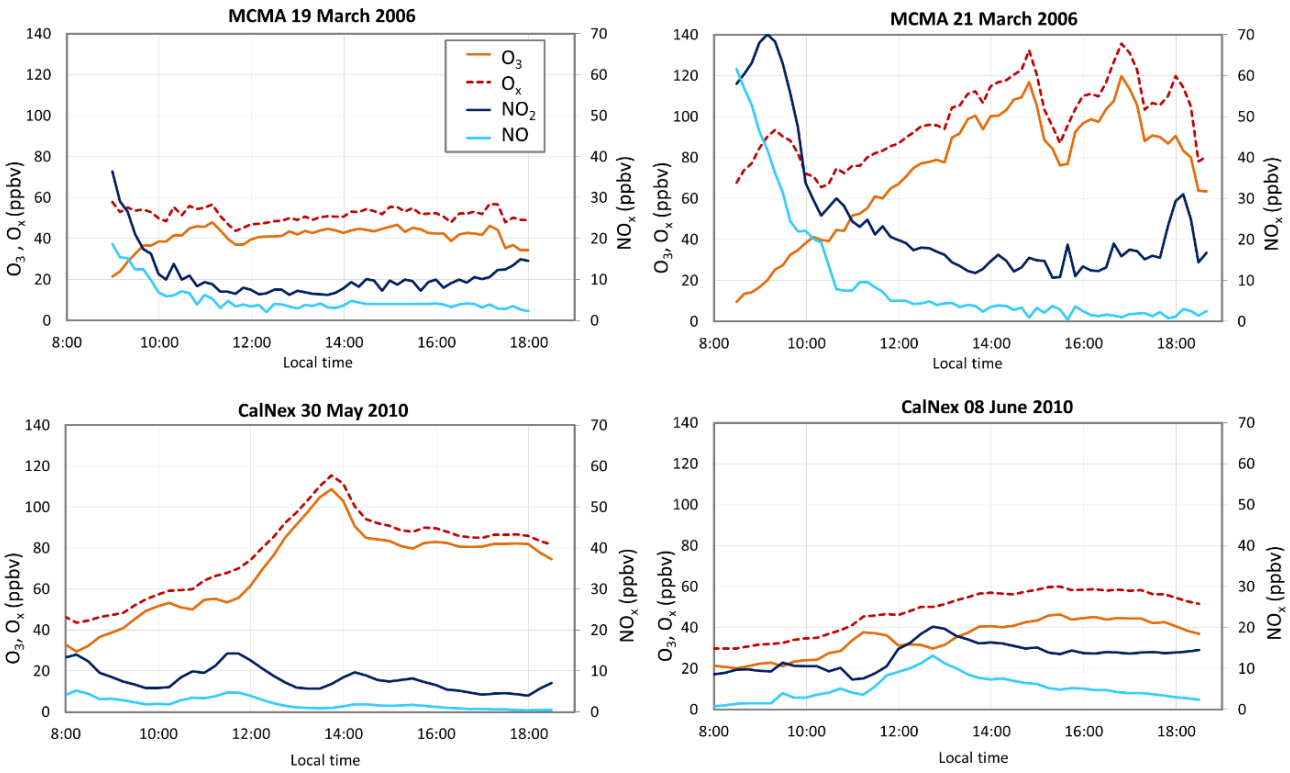

Figure S2. Ambient mixing ratios of O_3, NO_x and O_x for the selected days of the MCMA–2006 (top) and CalNex–2010 (bottom) campaigns.

S2.1 Quantification of photolysis frequencies under the UV filter

The absorption coefficient α of the Ultem film is linked to its light transmission:

$$I = I_0 e^{-ax} \quad (1)$$

where I and I_o are the transmitted and incident actinic fluxes, respectively, and x is the film thickness (0.25 mm) (Philipp et al., 1989). The actinic flux $I_o(\lambda)$ was calculated by the Tropospheric Ultraviolet-Visible model (TUV version 5.2) (Madronich and Flocke, 1999) for the selected days of the MCMA-2006 campaign and the transmission of the Ultem film was then calculated for each wavelength from Eq. (2), as shown in Fig. S3. J-values for NO_2, $O(^1D)$ and NO_3 were then calculated for clear sky conditions (ambient J-values) and for the UV filter (reference J-values) as:

$$Jvalue = \int_{\lambda_1}^{\lambda_2} I(\lambda)\, \sigma(\lambda)\, \varphi(\lambda)\, d\lambda \quad (2)$$

using the incident and transmitted actinic fluxes, respectively, the absorption cross section σ(λ) and the quantum yield φ(λ) for each molecule. For NO_3, both photolysis channels (producing $NO+O_2$ and NO_2+O) where examined separately.

The ratio between reference and ambient J-values provides a scaling transmission factor for each species (NO_2, $O_3 \rightarrow O(^1D)$ and NO_3). Chemical species photolyzed at wavelengths shorter than 400 nm were scaled using the scaling factor derived from $J(O^1D)$. Species photolyzed at wavelengths up to 450 nm (glyoxal, methylglyoxal, other α-carbonyl aldehydes and unsaturated dicarbonyls) were scaled using the scaling factor derived from $J(NO_2)$. Both channels of NO_3 photolysis lead to similar scaling factors with a difference <2%, and an average was used. The scaling factor of $J(NO_3)$ was used for the photolysis of O_3 leading to $O(^3P)$.

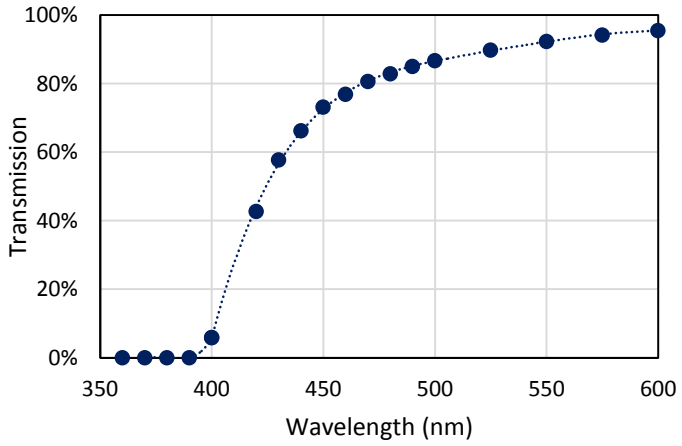

Figure S3. Transmission of light through the UV filter, 0.25 mm thick, as calculated by the absorption coefficient of polyetherimide (Ultem film).

S2.2 Modeling of the chemistry in the flow tubes

Table S2. Compounds constrained in the model for $P(O_3)_{amb}$

Species	Definition	Species	Definition
O3	Ozone	HC3	Alkanes, alcohols, esters and alkynes with OH rate constant (298 K, 1 atm) less than 3.4×10^{-12} cm^3 s^{-1}
SO2	Sulfur dioxide	HC5	Alkanes, alcohols, esters and alkynes with OH rate constant (298 K, 1 atm) between 3.4×10^{-12} $cm^3 s^{-1}$ and 6.8×10^{-12} cm^3 s^{-1}
CO	Carbon monoxide	HC8	Alkanes, alcohols, esters and alkynes with OH rate constant (298 K, 1 atm) greater than 6.8×10^{-12} cm^3 s^{-1}
H2	Hydrogen	OLT	Terminal alkenes
HONO	Nitrous acid	OLI	Internal alkenes
NO	Nitric oxide	TOL	Toluene and less reactive aromatics
NO2	Nitrogen dioxide	XYL	Xylene and more reactive aromatics
CH4	Methane	HCHO	Formaldehyde
ETH	Ethane	ALD	Acetaldehyde and higher aldehydes
ETE	Ehtene	API	α-pinene and other cyclic terpenes with one double bond
ISO	Isoprene	DIEN	Butadiene and other anthropogenic dienes
GLY	Glyoxal	KET	Ketones

Table S3. Photolytic reactions included in the model using their RACM notation. J-values scaling factors for the Reference flow tube. For a detailed explanation of the RACM notation see Stockwell et al. (1997).

Photolytic reaction	RACM symbol	Scaling factor	Value of sc. factor	Photolytic reaction	RACM symbol	Scaling factor	Value of sc. factor
$NO_2 \rightarrow NO+O(^3P)$	JNO2	JNO2	0.02	$CH_3OOH \rightarrow HO_2+OH+HCHO$	JOP1	JO1D	0
$O_3 \rightarrow O(^1D)+O_2$	JO1D	JO1D	0	$OP_2 \rightarrow HO_2+OH+ALD$	JOP2	JO1D	0
$O_3 \rightarrow O(^3P)+O_2$	JO3P	JNO3	0.82	$PAA \rightarrow CH_3O_2+OH$	JPAA	JO1D	0
$HONO \rightarrow HO+NO$	JHONO	JO1D	0	$KET \rightarrow ETHP+ACO3$	JKET	JO1D	0
$HNO_3 \rightarrow OH+NO_2$	JHNO3	JO1D	0	$GLY \rightarrow HCHO+CO$	JGLY1	JNO2	0.02
$HO_2NO_2 \rightarrow 0.65HO_2+ 0.65NO_2+0.35OH+0.35NO_3$	JHO2NO2	JO1D	0	$GLY \rightarrow CO+H_2$	JGLY2	JNO2	0.02
$NO_3 \rightarrow NO+O_2$	JNO3_NO	JNO3	0.82	$GLY \rightarrow HO_2+HO_2$	JGLY3	JNO2	0.02
$NO_3 \rightarrow NO_2+O(^3P)$	JNO3_NO2	JNO3	0.82	$MGLY \rightarrow HO_2+ACO+CO$	JMGLY	JNO2	0.02
$H_2O_2 \rightarrow OH+OH$	JH2O2	JO1D	0	$DCB \rightarrow TCO3+HO_2$	JDCB	JNO2	0.02
$HCHO \rightarrow HO_2+HO_2+CO$	JHCHO_CO	JO1D	0	$ONIT \rightarrow HO_2+NO_2+0.2ALD+0.8KET$	JONIT	JO1D	0
$HCHO \rightarrow CO+H_2$	JHCHO_H2	JO1D	0	$MACR \rightarrow CO+HO_2+ACO3+HCHO$	JMACR	JO1D	0
$ALD \rightarrow CH_3O_2+HO_2+CO$	JALD	JO1D	0	$HKET \rightarrow HO_2+ACO3+HCHO$	JHKET	JO1D	0

Table S4. Peroxy radical surrogates used for $p(O_3)$ calculations, and alkenes and organics used for $l(O_3)$ calculations. Peroxy radical outputs from the ambient atmospheric modeling were also used as model constraints for the flow tubes modeling.

	Species	Definition
Peroxy radicals used for $p(O_3)$ calculation	HO2	Hydroperoxy radical
	CH3O2	Methyl peroxy radical
	ETHP	Peroxy radical formed from ETH
	HC3P	Peroxy radical formed from HC3
	HC5P	Peroxy radical formed from HC5
	HC8P	Peroxy radical formed from HC8
	ETEP	Peroxy radical formed from ETE
	OLTP	Peroxy radical formed from OLT
	OLIP	Peroxy radical formed from OLI
	ISOP	Peroxy radical formed from ISO and DIEN
	APIP	Peroxy radical formed from API
	LIMP	Peroxy radical formed from LIM
	TOLP	Peroxy radical formed from TOL
	XYLP	Peroxy radical formed from XYL
	CSLP	Peroxy radical formed from CSL
	ACO3	Acetyl peroxy and higher saturated acyl peroxy radicals
	TCO3	Unsaturated acyl peroxy radicals
	KETP	Peroxy radicals formed from KET
	XO2	Accounts for additional NO to NO_2 conversions
Alkenes + Organics used for $l(O_3)$ calculation	ETE	Ethene
	OLT	Terminal alkenes
	OLI	Internal alkenes
	DIEN	Butadiene and other anthropogenic dienes
	ISO	Isoprene
	API	α-pinene and other cyclic terpenes with one double bond
	LIM	d-limonene and other cyclic diene-terpenes
	MACR	Methacrolein and other unsaturated monoaldehydes
	DCB	Unsaturated dicarbonyls
	TPAN	Unsaturated PANs

Table S5. Secondary compounds constrained in the model.

Species	Definition
N2O5	Dinitrogen pentoxide
H2O2	Hydrogen peroxide
CH3OOH	Methyl hydrogen peroxide
OP2	Higher organic peroxides
MGLY	Methylglyoxal and other α-carbonyl aldehydes
MACR	Methacrolein and other unsaturated monoaldehydes
UDD	Unsaturated dihydroxy dicarbonyl
HKET	Hydroxy ketone
DCB	Unsaturated dicarbonyls
ONIT	Organic nitrate
PAN	Peroxyacetyl nitrate and higher saturated PANs
TPAN	Unsaturated PANs
PAA	Peroxyacetic acid and higher analogs
ORA1	Formic acid
ORA2	Acetic acid and higher acids
HNO3	Nitric acid

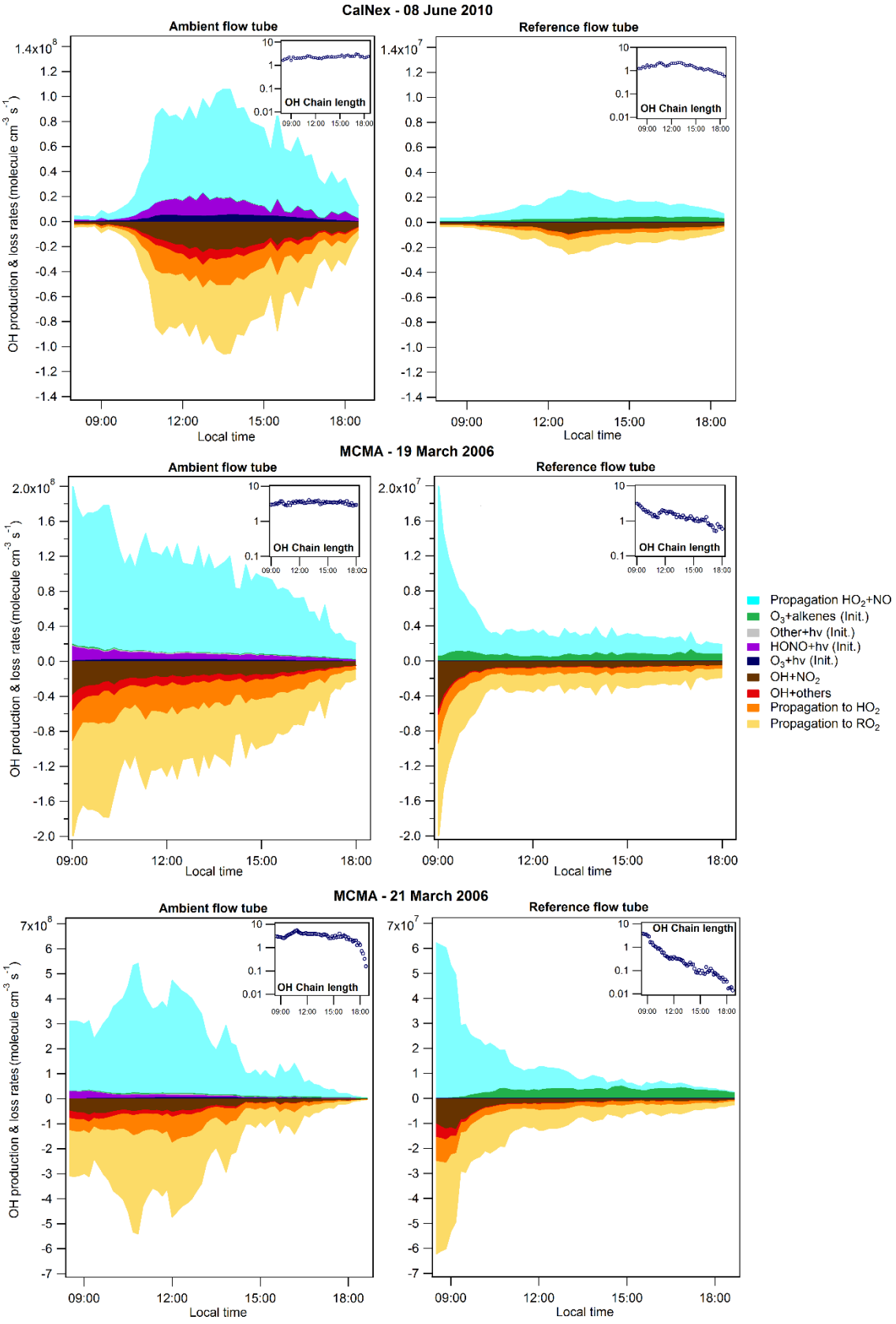

Figure S4. OH radical budgets for 08 May 2010 of CalNex–2010 (top), 19 March 2006 of MCMA–2006 (middle) and 21 March 2006 of MCMA–2006 (bottom). Radical budgets modeled for the ambient (left) and the reference (right) flow tubes. The OH chain length is also presented in an insert for each day and each flow tube. The note (Init.) in the legend indicates initiation reactions.

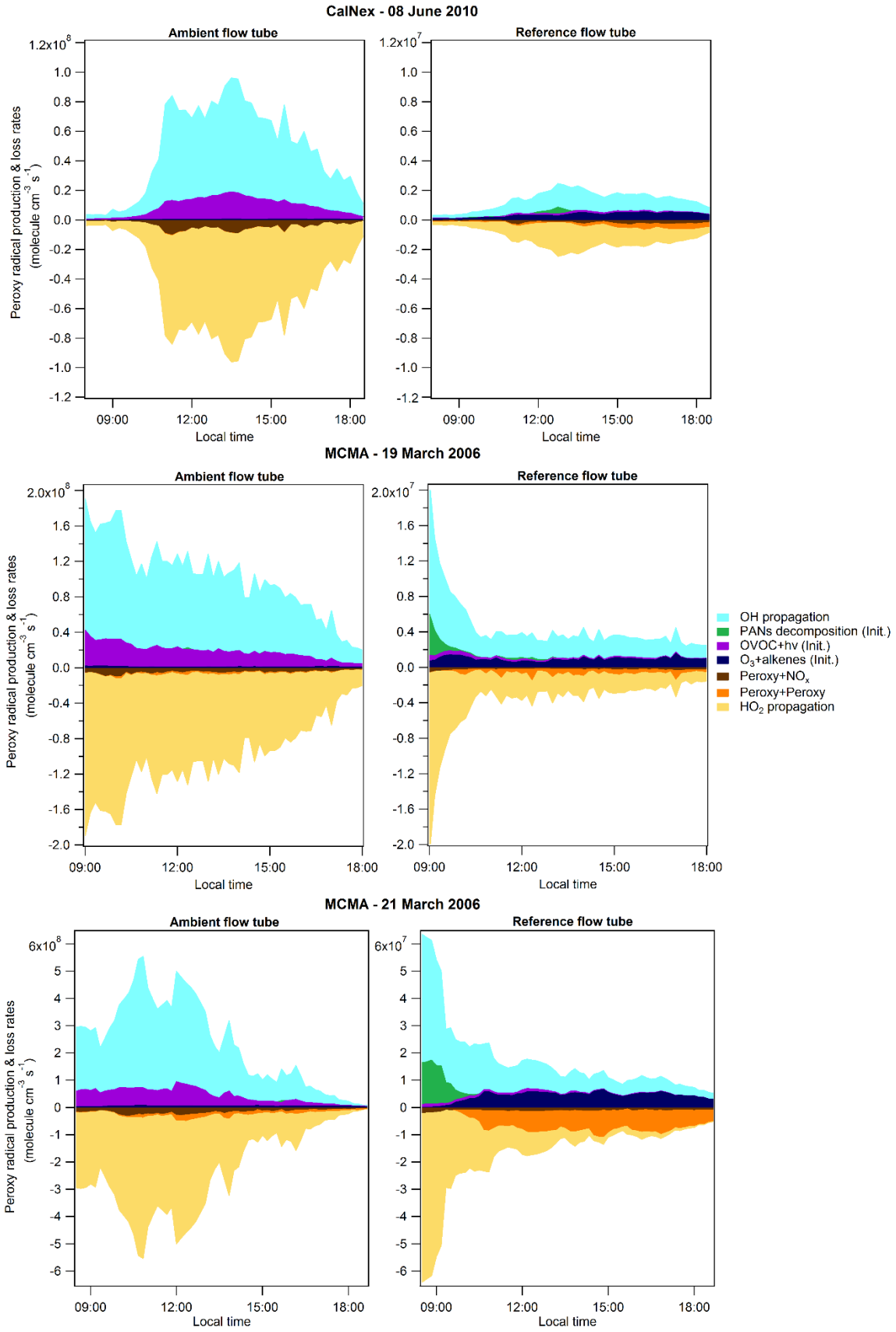

Figure S5. Total peroxy radical budgets for 8 May 2010 of CalNex–2010 (top), 19 March 2006 of MCMA–2006 (middle) and 21 March 2006 of MCMA–2006 (bottom). Radical budgets modeled for the ambient (left) and the reference (right) flow tubes. The note (Init.) in the legend indicates initiation reactions.

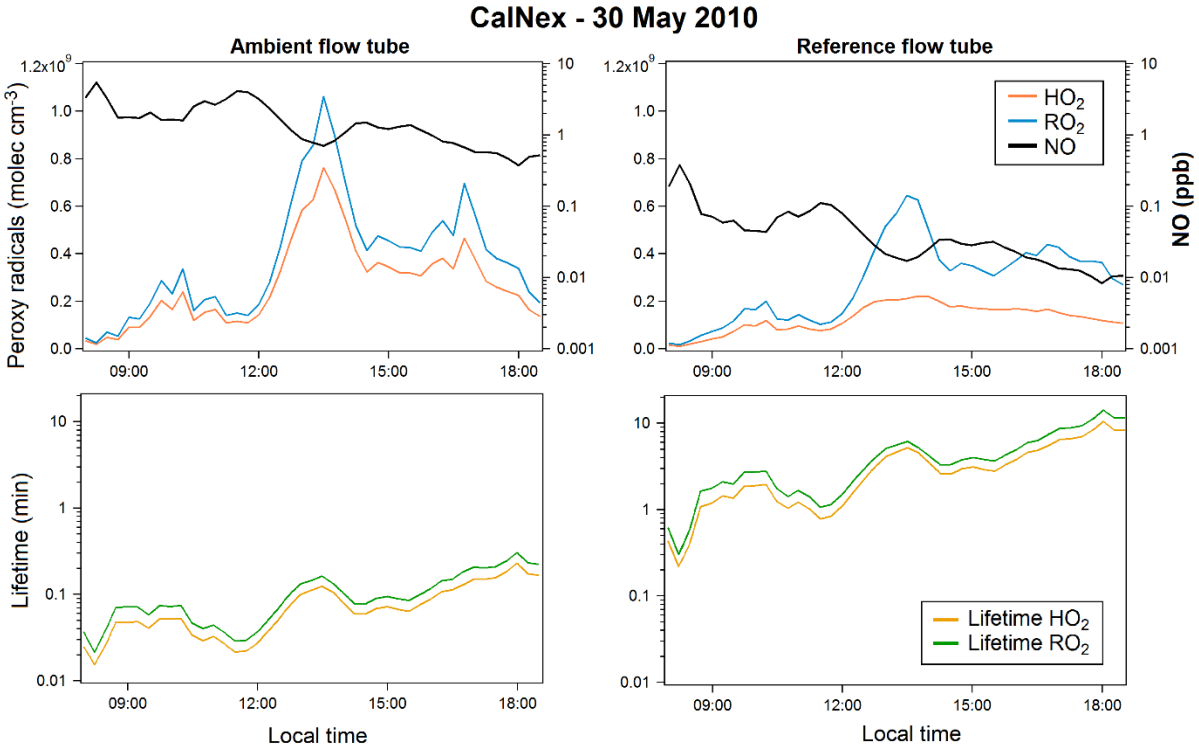

Figure S6. Peroxy radical concentrations, NO mixing ratios and lifetimes of HO_2 and RO_2 radicals in the ambient (left) and reference (right) flow tubes during 30 May 2010 of the CalNex–2010 campaign.

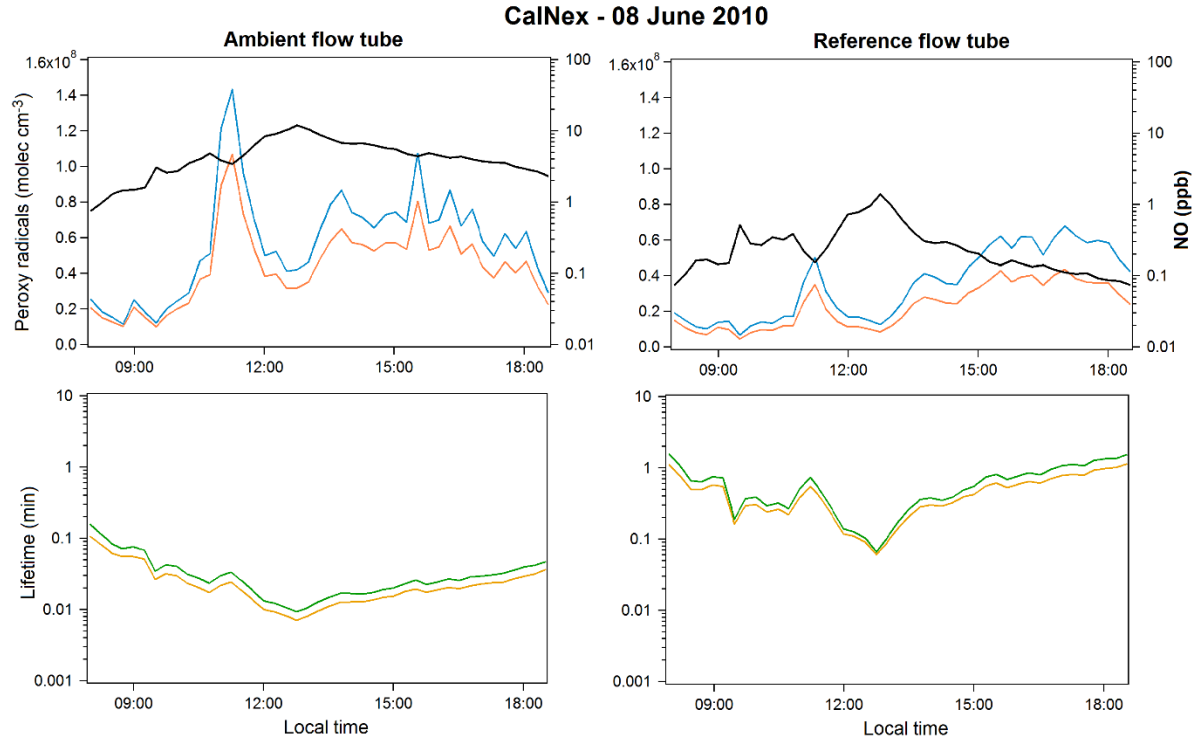

Figure S7. Peroxy radical concentrations, NO mixing ratios and lifetimes of HO_2 and RO_2 radicals in the ambient (left) and reference (right) flow tubes during 08 June 2010 of CalNex-2010.

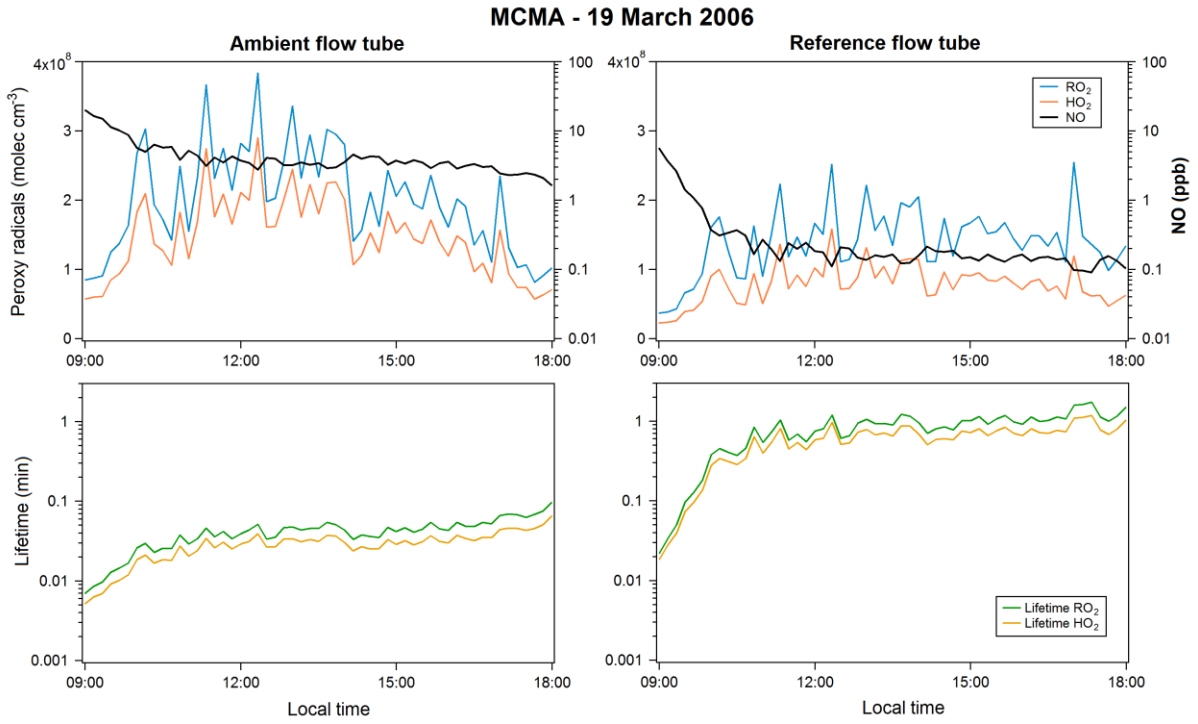

Figure S8. Peroxy radical concentrations, NO mixing ratios and lifetimes of HO_2 and RO_2 radicals in the ambient (left) and reference (right) flow tubes during 19 March 2006 of MCMA–2006.

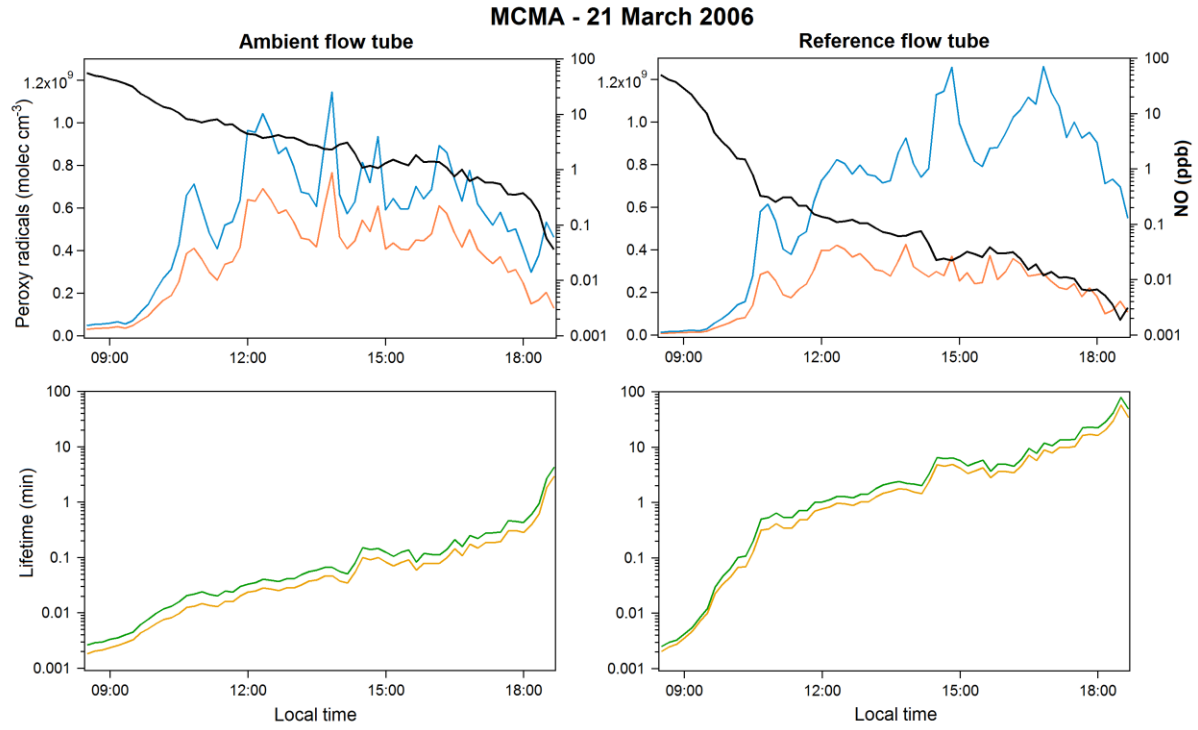

Figure S9. Peroxy radical concentrations, NO mixing ratios and lifetimes of HO_2 and RO_2 radicals in the ambient (left) and reference (right) flow tubes during 21 March 2006 of MCMA–2006.

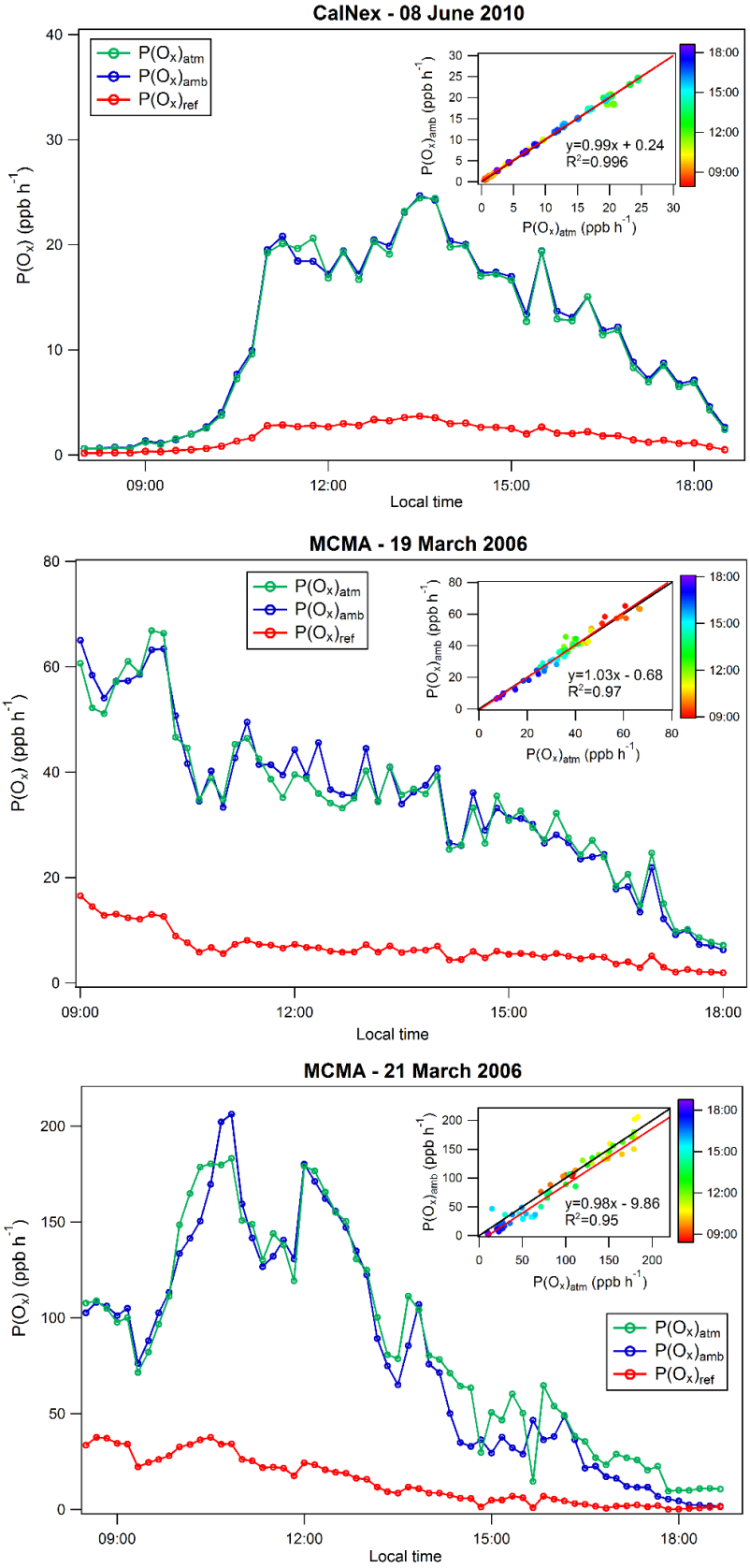

Figure S10. Modeled ozone production in the ambient atmosphere, $P(O_x)_{atm}$, in the ambient flow tube, $P(O_x)_{amb}$, and in the reference flow tube, $P(O_x)_{ref}$, on 08 May 2010 of CalNex–2010 (top), on 19 March 2006 of MCMA–2006 (middle) and on 21 March 2006 of MCMA–2006 (bottom). Insert plots show the correlation between $P(O_x)_{atm}$ and $P(O_x)_{amb}$, color-coded for the time of the day.

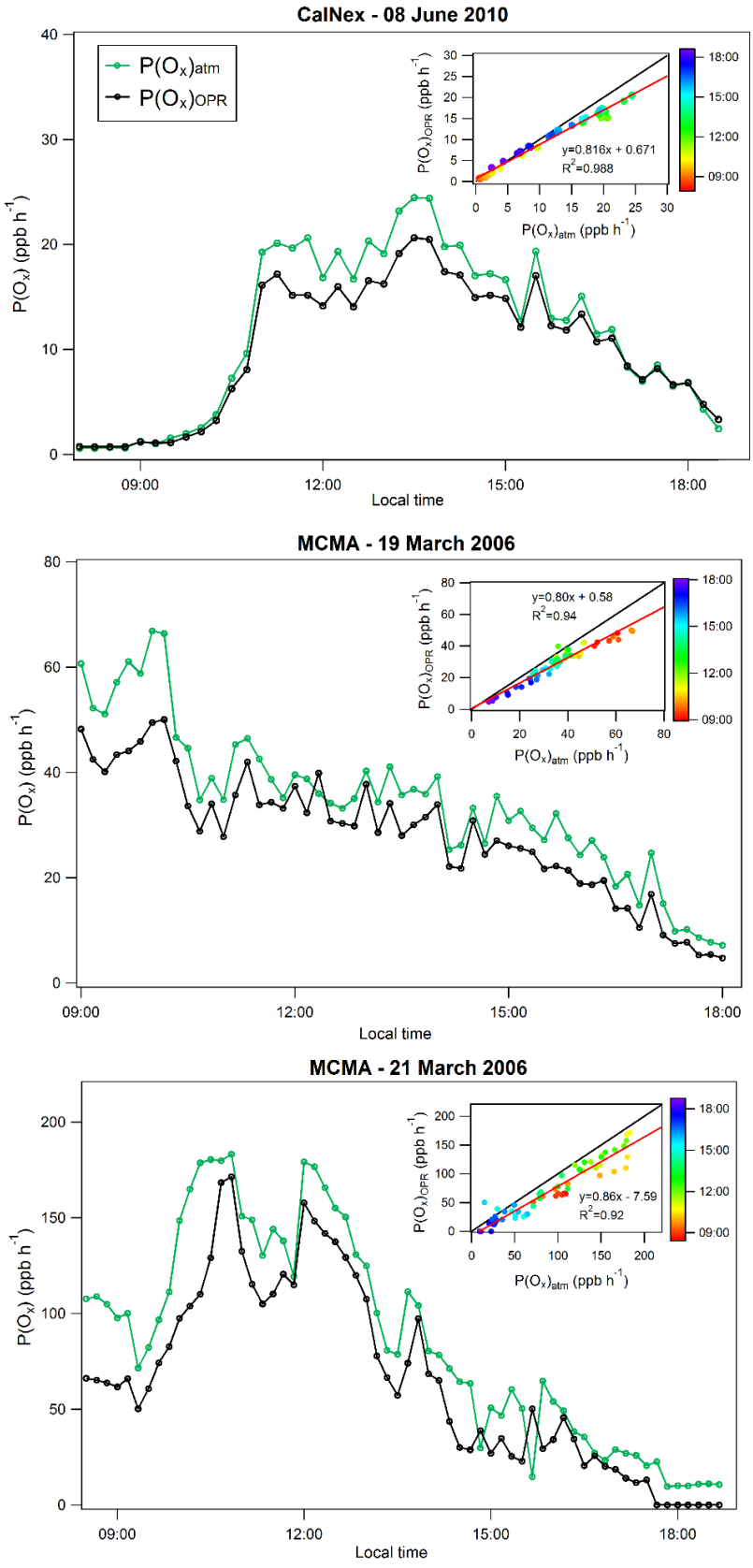

Figure S11. Modeled OPR ozone production, $P(O_x)_{OPR}$, and modeled ozone production in the ambient atmosphere, $P(O_x)_{atm}$, on 08 May 2010 of CalNex–2010 (top), on 19 March 2006 of MCMA–2006 (middle) and on 21 March 2006 of MCMA–2006 (bottom). Insert plots show the correlation between $P(O_x)_{atm}$ and $P(O_x)_{amb}$, color-coded for the time of the day.

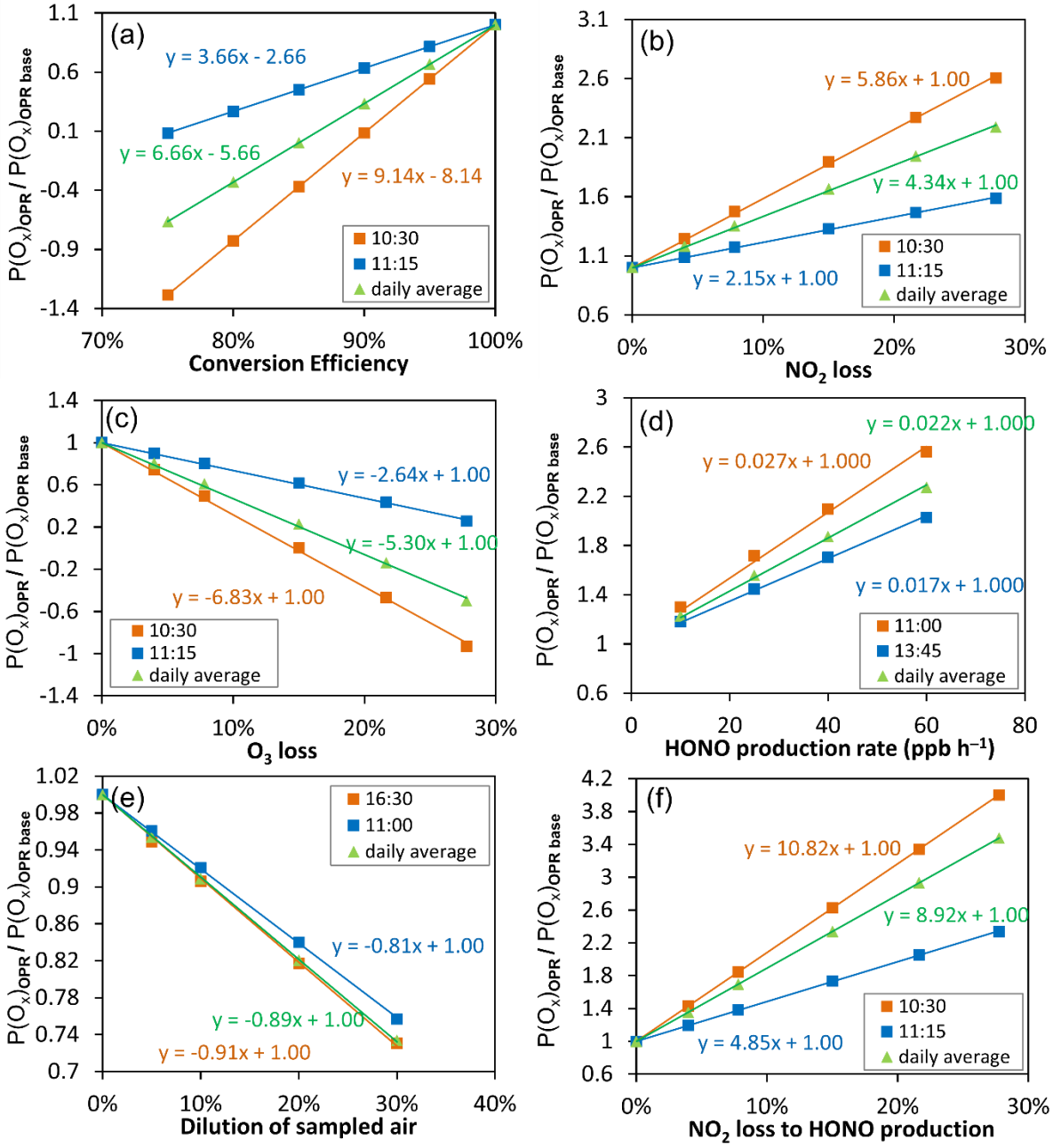

Figure S12. Sensitivity tests performed for 08 June 2010 (CalNex-2010) to assess the impact on $P(O_x)$ measurements of (a) the O_3-to-NO_2 conversion efficiency, (b) NO_2 and (c) O_3 dark losses, (d) heterogeneous HONO formation, (e) dilution of ambient air and (f) NO_2 loss towards HONO production in the flow tubes. The results presented here correspond to the two time periods of the day identified as lower and upper limits of the impact on the $P(O_x)$ measurements. The daily average behavior is also shown in green.

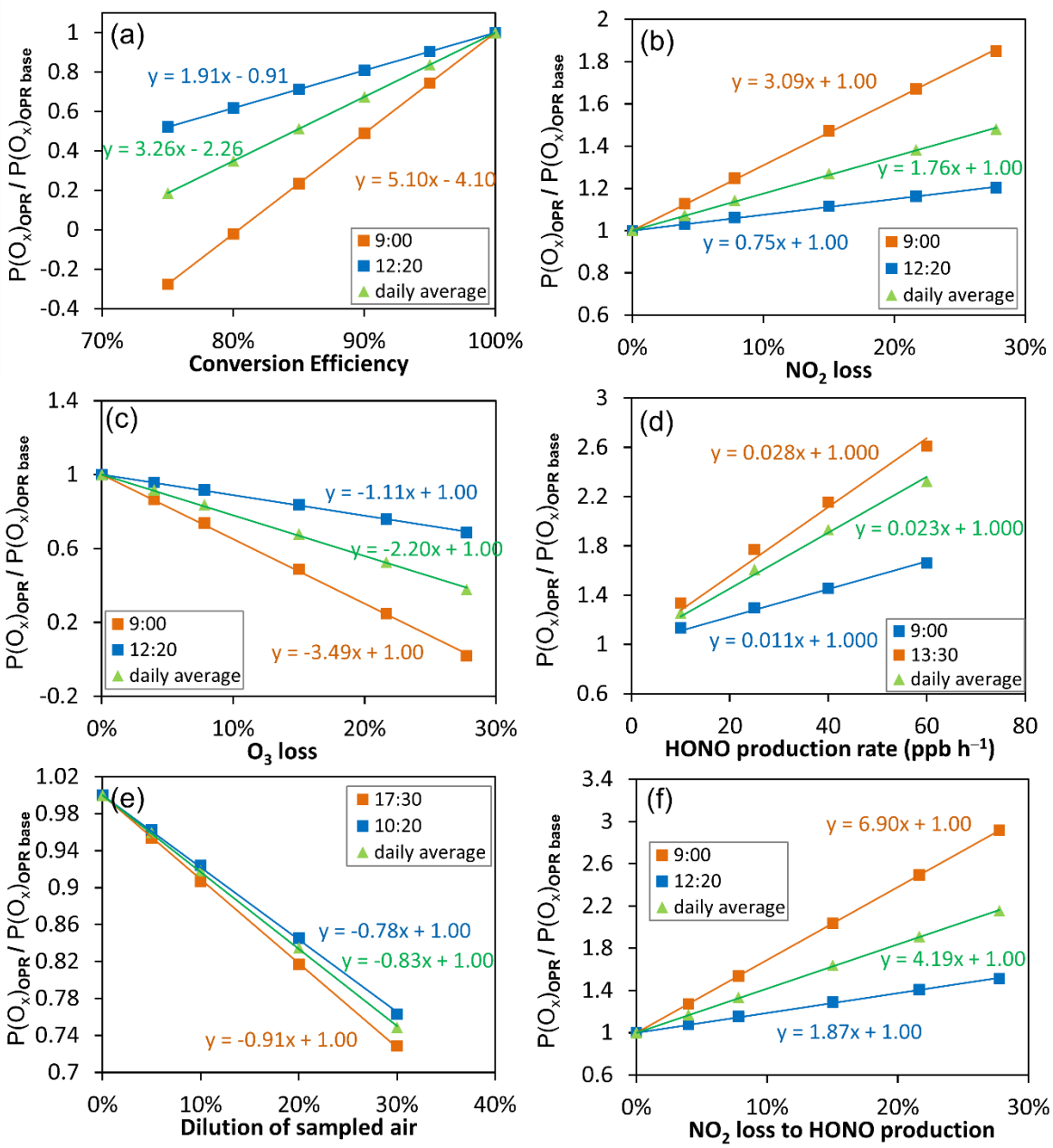

Figure S13. Sensitivity tests performed for 19 March 2006 (MCMA-2006) to assess the impact on $P(O_x)$ measurements of (a) the O_3-to-NO_2 conversion efficiency, (b) NO_2 and (c) O_3 dark losses, (d) heterogeneous HONO formation, (e) dilution of ambient air and (f) NO_2 loss towards HONO production in the flow tubes. The results presented here correspond to the two time periods of the day identified as lower and upper limits of the impact on the $P(O_x)$ measurements. The daily average behavior is also shown in green.

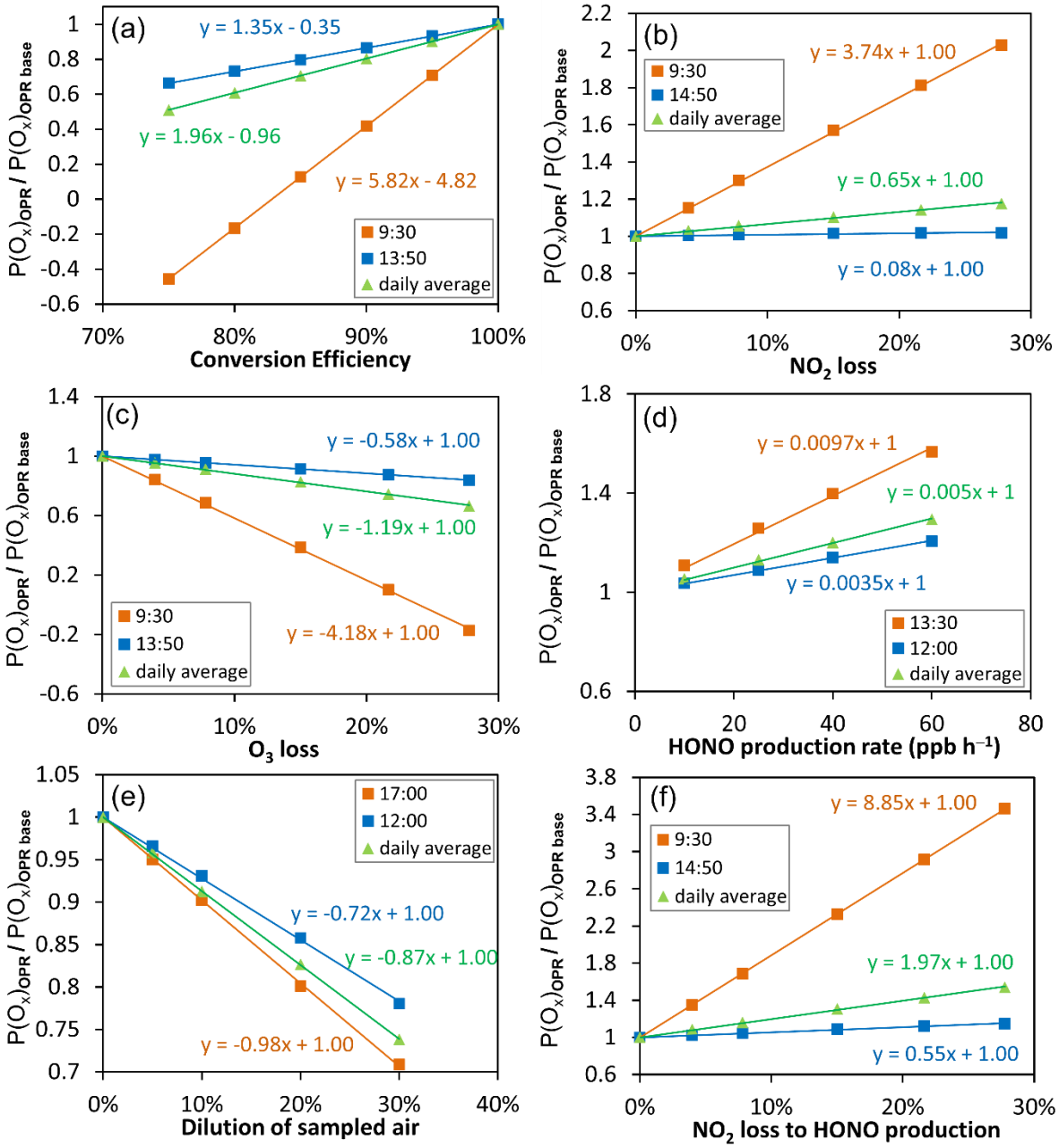

Figure S14. Sensitivity tests performed for 21 March 2006 (MCMA-2006) to assess the impact on $P(O_x)$ measurements of (a) the O_3-to-NO_2 conversion efficiency, (b) NO_2 and (c) O_3 dark losses, (d) heterogeneous HONO formation, (e) dilution of ambient air and (f) NO_2 loss towards HONO production in the flow tubes. The results presented here correspond to the two time periods of the day identified as lower and upper limits of the impact on the $P(O_x)$ measurements. The daily average behavior is also shown in green.

References

Madronich, S., and Flocke, S.: The Role of Solar Radiation in Atmospheric Chemistry, in: Environmental Photochemistry, edited by: Boule, P., The Handbook of Environmental Chemistry, Springer Berlin Heidelberg, 1-26, 1999.

Philipp, H. R., Le Grand, D. G., Cole, H. S., and Liu, Y. S.: The optical properties of a polyetherimide, Polymer Engineering & Science, 29, 1574-1578, 1989.

Stockwell, W. R., Kirchner, F., Kuhn, M., and Seefeld, S.: A new mechanism for regional atmospheric chemistry modeling, Journal of Geophysical Research: Atmospheres, 102, 25847-25879, 1997.